

## X-RAY AND OPTICAL EMISSION FROM RADIO HOT SPOTS OF POWERFUL QUASARS

F. TAVECCHIO, R. CERUTTI, AND L. MARASCHI  
INAF–Osservatorio Astronomico di Brera, via Brera 28, 20121 Milano, Italy

R. M. SAMBRUNA AND J. K. GAMBILL  
George Mason University, Fairfax, VA 22030

C. C. CHEUNG<sup>1</sup>  
Center for Space Research, Massachusetts Institute of Technology, 77 Massachusetts Avenue, Cambridge, MA 02139

AND

C. MEGAN URRY  
Department of Astronomy, Yale University, New Haven, CT 06520  
*Received 2005 February 7; accepted 2005 May 25*

### ABSTRACT

In a survey with *Chandra* and *HST* of a sample of 17 radio sources with bright radio jets (16 powerful FR II and one nearby FR I), we detected X-ray and optical emission from a number of radio hot spots and lobes. Six hot spots on the near sides of powerful FR II galaxies (as determined from the jet asymmetry) were detected at X-rays, while none were detected on the far side, suggesting that high-energy emission from hot spots is anisotropic. In the nearby FR I galaxy 0836+299 (the only FR I in our sample) both hot spots are detected in X-rays, in agreement with the symmetric radio morphology. In the latter case the spectral energy distributions (SEDs) of both hot spots can be modeled from radio to X-rays with synchrotron emission from a single power-law energy distribution of electrons with Lorentz factors up to  $\sim 2 \times 10^7$ . For the six hot spots of powerful FR II galaxies the X-ray flux lies above the extrapolation from the radio-to-optical continuum. Modeling the SEDs with a one-zone synchrotron self-Compton model, we find that equipartition is strongly violated, with the particle energy density dominating over the magnetic field one by 1–2 orders of magnitude. We discuss alternatives to this simple model, concluding that a viable alternative is that the X-ray emission is produced in the still-relativistic (Doppler factor  $\delta = 3$ –6) terminal part of the jet by inverse Compton (IC) scattering on the CMB or synchrotron photons emitted by plasma flowing with a small velocity. X-ray emission from some of the lobes is detected on the side opposite to the jet, suggesting the possible relevance of back-scattered central radiation in providing seed photons for the IC process.

*Subject headings:* galaxies: active — quasars: general — X-rays: galaxies

### 1. INTRODUCTION

The study of relativistic jets (and of radio sources in general) advanced significantly in recent years thanks to the advent of the excellent sensitivity and spatial resolution of the *Chandra X-Ray Observatory*, which allowed the study of their multiwavelength emission properties to be extended into the X-ray band. In fact, in those sources where the X-rays are interpreted as being due to the inverse Compton (IC) process, it is possible to break the degeneracy of the parameters that is present when only the synchrotron component is visible. In this case we can test whether the hypothesis of equipartition, usually adopted to obtain values for the physical properties of jets, lobes, and hot spots, is valid.

In the past, only a few hot spots were detected in the X-ray band at the limited sensitivities of *Einstein*, *Röntgensatellit* (*ROSAT*), and the *Advanced Satellite for Cosmology and Astrophysics* (*ASCA*). The best case was that of the hot spots detected by *ROSAT* in the archetypal FR II radio galaxy Cygnus A (Harris et al. 1994), for which the bright X-ray emission, readily interpreted as synchrotron self-Compton (SSC) radiation, allowed firm constraints to be put on the physical state of the plasma. In particular, it was confirmed that the Cyg A hot spots are close to the equipartition condition. In addition, X-ray emission from the lobes of some nearby radio galaxies (PKS 1343–601, Fornax A) was detected

with *ASCA* and interpreted in terms of IC scattering of cosmic microwave background (CMB) photons (Tashiro et al. 1998, 2001), confirming previous *ROSAT* findings (Feigelson et al. 1995). The determination of the conditions within the hot spots is important especially for understanding the physical processes associated with the collision of the jet with the intergalactic medium (Blandford & Rees 1974; Scheuer 1974; Begelman & Cioffi 1989; Cox et al. 1991; Kino & Takahara 2004).

After Cyg A, several other hot spots have been detected in the X-ray band in radio galaxies. For a large number of them, the emission can be simply described by the SSC process, with parameters very near the equipartition condition (e.g., Harris & Krawczynski 2002). However, a nonnegligible number of hot spots emit X-rays at a level far above that predicted by the SSC process under the equipartition hypothesis. The discrepancy is too large to be reconciled with uncertainties on the parameters, yielding magnetic fields largely below equipartition values. On the other hand, due to the lack of data in the optical, in several instances the alternative possibility that the X-ray flux is just the high-energy tail of the synchrotron emission cannot be excluded (see Hardcastle et al. 2004 for a review).

During our systematic study of optical and X-ray emission from large-scale jets in a sample of radio sources (Sambruna et al. 2004, hereafter Paper I), we obtained a new set of X-ray, optical, and radio observations of hot spots and lobes in 16 powerful FR II radio galaxies and one nearby low-power radio galaxy. Several of the hot spots detected at X-rays also have an

<sup>1</sup> Jansky Postdoctoral Fellow; National Radio Astronomy Observatory.

TABLE 1  
SUMMARY OF THE DETECTIONS IN THE JET OF OUR SAMPLE

SOURCE	JET			COUNTERJET			HOT SPOT			COUNTER-HOT SPOT			LOBE			COUNTERLOBE		
	r	o	x	r	o	x	r	o	x	r	o	x	r	o	x	r	o	x
0405–123 .....	Y	...	...	...	...	...	Y	Y	Y	Y	...	...	Y	...	...	Y	...	...
0605–085 .....	Y	...	Y	...	...	...	*	...	...	...	...	...	...	...	...	...	...	...
0723+679 .....	Y	Y	Y	...	...	...	Y	...	Y	...	...	...	Y	...	...	Y	...	Y
0802+103 .....	Y	...	...	...	...	...	Y	...	...	...	...	...	Y	...	...	Y	...	...
0836+299 .....	Y	...	...	Y	...	...	Y	Y	Y	Y	...	Y	Y	...	...	Y	...	...
0838+133 .....	Y	Y	Y	...	...	...	Y	...	Y	...	...	...	Y	...	...	Y	...	Y
1040+123 .....	Y	Y	Y	...	...	...	Y	Y	Y	...	...	...	Y	...	...	Y	...	Y
1055+018 .....	Y	...	...	...	...	...	...	...	...	...	...	...	Y	...	...	Y	...	...
1136–135 .....	Y	Y	Y	...	...	...	Y	Y	...	Y	...	...	Y	...	...	Y	...	Y
1150+497 .....	Y	Y	Y	...	...	...	Y	Y	Y	...	...	...	Y	...	...	Y	...	...
1354+195 .....	Y	Y	Y	...	...	...	Y	...	Y	Y	...	...	...	...	...	Y	...	...
1510–089 .....	Y	Y	Y	...	...	...	...	...	...	...	...	...	Y	...	...	Y	...	...
1641+399 .....	Y	Y	Y	...	...	...	...	...	...	...	...	...	Y	...	...	Y	...	...
1642+690 .....	Y	Y	Y	...	...	...	Y	...	...	...	...	...	Y	...	...	Y	...	...
1741+279 .....	Y	...	...	...	...	...	Y	...	...	...	...	...	Y	...	...	Y	...	...
1928+738 .....	Y	Y	Y	Y	...	...	Y	...	...	...	...	...	Y	...	...	Y	...	...
2251+134 .....	Y	Y	Y	...	...	...	Y	Y	...	Y	...	...	Y	...	...	Y	...	...

NOTE.—Y = detection; the asterisk indicates a hot spot misclassified as a knot in Paper I.

optical counterpart, providing better constraints to the spectral energy distributions (SEDs) and the models. The multiwavelength observations of the jets are discussed in Paper I. Here, we focus on the emission properties of the jet terminal features.

The paper is structured as follows. In § 2 we present the sample, the adopted definitions for the lobes and hot spots, and the derived data. The SEDs are presented and modeled in § 3. Discussion and a conclusion follow in § 4. Throughout this work we use the current *Wilkinson Microwave Anisotropy Probe* (*WMAP*) cosmological parameters:  $H_0 = 71 \text{ km s}^{-1} \text{ Mpc}^{-1}$ ,  $\Omega_\Lambda = 0.73$ , and  $\Omega_m = 0.24$  (Bennett et al. 2003).

## 2. THE SAMPLE

As discussed in Paper I, the jet survey sample is biased toward beaming because of the selection criteria. The sample contains 17 sources, of which 16 are classified as quasars with powerful radio jets and an FR II morphology, while the low-power radio galaxy 0836+299 is classified as an FR I on the basis of the overall morphology and power. We note, however, that the presence of hot spots in this class of radio galaxies is unusual. Basic properties of the targets are listed in Table 1 of Paper I.

The specific aim of the survey was to study the origin of the X-ray and optical emission from the jets. As a bonus, we also obtained a number of X-ray and optical detections of the jets' terminal radio features: hot spots and lobes. Here, we adopt the empirical definition of lobes by Bridle et al. (1994): a lobe region refers to any remaining radio emission (generally diffuse) not contained in the jet. For the hot spots, we extend the Bridle definition and classify as a hot spot every compact bright feature located *at or beyond the end of the jet*; the jet end is determined by any of the following: (1) disappearance of the jet emission, (2) an abrupt change of direction ( $\gtrsim 30^\circ$  within a distance equal to the jet width) for the jet emission, or (3) a decollimation of the emission by more than a factor of 2. The original Bridle definition requires a feature to be embedded within the lobe emission to be classified as a hot spot. Our revised definition is motivated by the cases in which bright features associated with the end of the jet are observed, but without a clear detection of diffuse (radio) emission associated with the lobe, the latter most

likely being due to a combination of the low surface brightness of these structures with the relatively large flux threshold of our radio observations. Note that the definitions we use in this work differ from the broad definition of “lobes” used in Paper I, which included hot spots as part of the lobes.

Table 1 summarizes the detections in the radio, optical, and X-ray bands of jets, counterjets, hot spots, counter-hot spots, lobes, and counterlobes (the prefix “counter” indicates the side of the source opposite to the jet). For each feature a “Y” indicates a detection in a given band. The bias favoring beamed sources is apparent from the fact that almost all the radio jets are one sided (only in two sources, 1928+738 [Hummel et al. 1992] and the FR I 0836+299 [van Breugel et al. 1986], is there any evidence of a counterjet).

Focusing on the features discussed in this work, inspection of Table 1 reveals two striking trends: (1) no counter-hot spot is detected at optical or X-ray wavelengths (except, again, for the peculiar case of 0836+299); and (2) we do not detect X-ray emission from lobes, while four counterlobes are marginally detected. The first point is quite interesting, since it suggests that beaming is involved to some extent also in the optical and X-ray emission from the hot spots. As already noted in Paper I, the second result is in agreement with the back-scattering model of Brunetti et al. (1997), which naturally predicts a more luminous X-ray emission from the counterlobe with respect to the lobe. Due to the short exposures, the data for the lobes are of insufficient quality to allow a more quantitative analysis.

We restrict our analysis to the sources where the hot spots are detected at X-rays; for all of them (see Table 1) we have also optical information, either a detection or a stringent upper limit to the optical flux. The multiwavelength fluxes used here have been presented in Paper I, to which we refer the reader for details on the data reduction and analysis and for X-ray images and radio overlays.

The resulting subsample includes 0405+123 A, 0836+299 B, 1040+123 D, and 1150+497 H (detected in three bands); and 0723+679 D, 0838+133 C, and 1354+195 I (optical upper limits). Contamination due to line-emitting gas prevents us from constraining the upper limit for 0836+299 C.

TABLE 2  
SUMMARY OF THE OBSERVATIONAL PARAMETERS OF THE HOT SPOTS ANALYZED IN THIS WORK

Source	$z$	Hot Spot	$F_{5 \text{ GHz}}$ (mJy)	$\alpha_r$	$F_{5852 \text{ \AA}}$ ( $\mu\text{Jy}$ )	$F_{1 \text{ keV}}$ (nJy)
0405–123 .....	0.574	A	$204 \pm 20$	$0.90 \pm 0.10$	$0.58 \pm 0.05$	$1.6 \pm 0.5$
0723+679 .....	0.846	D	$110 \pm 11$	$0.79 \pm 0.07$	$<0.07$	$1.3 \pm 0.4$
0838+133 .....	0.684	C	$110 \pm 11$	$0.74 \pm 0.08$	$<0.08$	$0.7 \pm 0.2$
1040+123 .....	1.029	D	$222 \pm 22$	$0.87 \pm 0.08$	$0.02 \pm 0.01$	$0.7 \pm 0.3$
1150+497 .....	0.334	H	$74 \pm 7$	$0.81 \pm 0.08$	$0.05 \pm 0.02$	$1.8 \pm 0.5$
1354+195 .....	0.720	I	$87 \pm 9$	$0.92 \pm 0.07$	$<0.07$	$1.0 \pm 0.4$
0836+299 .....	0.064	B	$18 \pm 2$	$0.85 \pm 0.11$	$0.91 \pm 0.1$	$2.2 \pm 0.6$
0836+299 .....	...	C	$14 \pm 1.5$	$0.85 \pm 0.11$	... <sup>a</sup>	$0.7 \pm 0.2$

NOTE.—Radio (in units of mJy), optical (in units of  $\mu\text{Jy}$ ), and X-ray fluxes (in units of nJy) were extracted in circular regions of  $1''$ , and  $\alpha_r$  is the radio spectral index for the hot spots considered in this work.

<sup>a</sup> No upper limit can be placed on the optical emission, since the emission is expected to be diffuse.

The alphabetic letters refer to the label of the relevant feature in the images presented in Paper I. For these features, additional multifrequency radio data (in the 1.4–1.7 GHz band and at 5 and 22 GHz) using the Multielement Radio-linked Interferometer Network (MERLIN) and the Very Large Array (VLA) were collected (Cheung 2004; C. C. Cheung et al., in preparation). Radio spectral indices (typical errors  $\pm 0.1$ ) and some structural information derived from the latter data are used here in advance of publication.

### 3. SPECTRAL ENERGY DISTRIBUTIONS

For convenience, the fluxes used and the recently determined radio spectral indices (Cheung 2004) are reported in Table 2. Figure 1 illustrates the SEDs of the eight hot spots suitable for multiwavelength analysis. The fluxes were measured from extraction regions with  $1''$  radii. Also shown (*open circles*) are the radio fluxes of the most compact component resolved by

the VLA (not shown for 1150+497 and 1354+195, since their hot spots are already resolved at  $1''$  resolution). From Figure 1 it is apparent that for the six “one-sided” hot spots (0405–123 A, 0723+679 D, 0838+133 C, 1040+123 D, 1150+497 H, and 1354+195 I) it is not possible to model the continuum from the radio to the X-rays with a single power law. The SEDs of the two symmetrical hot spots, 0836+299 B and 0836+299 C, can instead be reproduced by a single power law: the latter case will be discussed separately (§ 3.3).

We stress the importance of good quality optical data (detections or upper limits) for the analysis of the multifrequency SEDs. For instance, two of the hot spots belonging to our set (0723+679 D and 0838+133 C) are also present in the sample discussed in the recent paper by Hardcastle et al. (2004). For these two sources Hardcastle et al. (2004), using filtered snapshot Wide Field Planetary Camera 2 (WFPC2) exposures, obtain optical upper limits consistent with a single power-law SED. The upper limits obtained from our unfiltered Space Telescope Imaging Spectrograph (STIS) observations are deeper, and the corresponding fluxes exclude a single power law in the SED.

In the following discussion, we assume that the concave SEDs originate from the contribution of two emission processes, synchrotron at low frequencies and inverse Compton scattering at high energies. Possible alternatives will be considered in § 4.

#### 3.1. Reproducing the SEDs of Quasars’ Hot Spots with the Synchrotron + IC Model at Rest

We reproduced the observed radio, optical, and X-ray fluxes using a simple *one-zone* synchrotron + IC model (for a description, see Tavecchio et al. 2000). The source is modeled as a homogeneous sphere with radius  $R$ , filled by relativistic electrons with a power-law energy distribution with index  $n$ ,  $N(\gamma) = K\gamma^{-n}$ , within the two limits  $\gamma_{\min}$  and  $\gamma_{\max}$ , and by magnetic field  $B$ . For a  $1''$  emission region the energy densities of synchrotron photons and of the CMB can be comparable. Thus, both contributions to the IC process have been taken into account.

The slope of the electron distribution is fixed at the value inferred from the slope of the radio spectrum,  $n = 2\alpha_r + 1$ . Since we assume a single power-law spectrum, the limit  $\gamma_{\max}$  is determined by the cutoff in the synchrotron spectrum, which must satisfy the optical flux or upper limit. In general, a wide range of  $\gamma_{\min}$  is consistent with the data: we chose to minimize the discrepancy with equipartition. This leads to relatively large values of  $\gamma_{\min} \sim 500\text{--}10^3$ . For large values of the magnetic field, such as those required for extremely small sizes of the sources (see below), the maximum value for  $\gamma_{\min}$  can also be limited by the

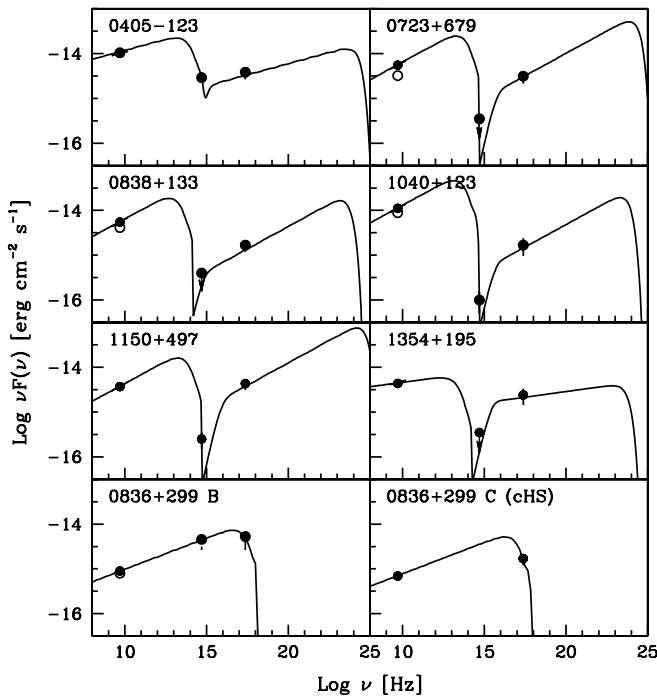


FIG. 1.—SEDs of our hot spot sample. Filled and empty circles report the fluxes extracted within circles of  $1''$  and within the VLA circle (but for the cases of 1150+497 and 1354+195, see text), respectively. The solid line reports the model calculated with the beamed synchrotron and IC/CMB emission (see text for details).

TABLE 3  
PARAMETERS FOR THE SYNCHROTRON + SSC + IC/CMB MODEL

Source (1)	Hot Spot (2)	$R$ ( $10^{22}$ cm) (3)	$n$ (4)	$K$ ( $\text{cm}^{-3}$ ) (5)	$\gamma_{\min}$ (6)	$\gamma_{\max}$ ( $\times 10^5$ ) (7)	$\delta$ (8)	$B$ ( $\mu\text{G}$ ) (9)	$B_{\text{eq}}$ ( $\mu\text{G}$ ) (10)
0405–123 .....	A	2.0	2.8	0.6	350	13	1	11.5	85
		2.0	2.8	$1.8 \times 10^{-4}$	7	3.5	5	30	...
0723+679 .....	D	2.3	2.6	0.15	300	8	1	8.5	80
		2.3	2.6	$6.8 \times 10^{-5}$	16	4	5	20	...
0838+133 .....	C	2.1	2.6	0.07	350	8	1	10.5	71
		2.1	2.6	$5. \times 10^{-5}$	5	3	4.5	25	...
1040+123 .....	D	2.4	2.6	0.055	600	4	1	26	96
		2.4	2.6	$2.5 \times 10^{-4}$	20	3	3.5	35	...
1150+497 .....	H	1.4	2.6	0.17	400	9	1	3.5	52
		1.4	2.6	$1.8 \times 10^{-5}$	15	4.5	6.6	10	...
1354+195 <sup>a</sup> .....	I	3.2	2.8	0.52	500	2	1	4.5	50
		3.2	2.8	$3.5 \times 10^{-4}$	12	2	4.5	27	...
0836+299 .....	B	0.37	2.7	$9 \times 10^{-4}$	10	260	1	75	...
0836+299 .....	C	0.37	2.7	$8.6 \times 10^{-4}$	10	180	1	70	...

NOTES.—First row for each source shows parameters assuming the hot spot is at rest, and the second row, assuming equipartition with relativistic motion of the hot spot. Col. (1): Source IAU name. Col. (2): Feature broadband detected. Col. (3): Source radius  $R$ . Col. (4): Power-law index of the electron energy distribution. Col. (5): Electron density in  $e^- \text{cm}^{-3}$ . Col. (6): Minimum electron Lorentz factor. Col. (7): Maximum electron Lorentz factor. Col. (8): Doppler factor. Col. (9): Magnetic field. Col. (10): Equipartition magnetic field.

<sup>a</sup>  $R = 1''$ .

low-energy synchrotron break, located at  $\nu_{\min} \sim 3 \times 10^6 B \gamma_{\min}^2$ , which must fall below the minimum observed radio frequency.

Assuming  $R \simeq 1''$  (corresponding to linear sizes in the range 5–8 kpc), the model yields the parameters reported in Table 3 (and the model for the specific case of 0405–123 A is shown in Fig. 2a). The inferred magnetic field,  $B$ , can be compared with the equipartition field, directly estimated from the radio flux,  $B_{\text{eq}}$  (see Appendix A). Even assuming in each case the maximum  $\gamma_{\min}$  allowed by the data ( $\gamma_{\min} \sim 400\text{--}10^3$ ), which minimizes the particle energy density, the ratio  $B_{\text{eq}}/B$  spans the range 3–20, indicating that equipartition is strongly violated in all the sources. We note that for 0723+679 and 0838+133 our results are consistent with those found in a similar analysis by Hardcastle et al. (2004), despite their weaker constraint on  $\gamma_{\min}$  due to the less stringent optical upper limit.

On the other hand, due to the limited resolution of *Chandra*, the size of the emission region is uncertain. In fact, high-resolution radio maps indicate deviations from homogeneity: in most sources an unresolved region is surrounded by diffuse emission (in some cases providing a nonnegligible fraction of the radio flux), while in other cases substructures are revealed (e.g., the 1150+497 hot spot is resolved in three different compact components). We therefore repeated the modeling with sizes given by the most compact region visible in the high-frequency radio maps ( $\sim 0''.2$ ; an example is reported in Fig. 2b). In the case of 1150+497, we assumed that the X-ray emission is equally shared between the three subcomponents and modeled one of them. We did not consider 1354+195, since the hot spot in this source is already extended at the *Chandra* resolution.

Decreasing the radius of the emission region causes the radiation density  $U_{\text{rad}}$  to increase (as  $R^{-2}$ ), and to keep the Compton-to-synchrotron luminosity ratio to observed values,  $U_B$  increases too, as expected. However, the equipartition field also grows with decreasing radius. The combined effect is that the violation of equipartition is reduced but only in a minor way for changes in size of factors of a few.

We note that the major uncertainty in the derived physical parameters comes from the basic assumptions of the modeling. The errors on the observational quantities, such as the fluxes

and the radio spectral slopes, introduce small variations on the derived quantities that do not affect the results of our study.

In conclusion, if the emitting plasma is at rest, the magnetic energy density derived using the SSC process and IC scattering on the CMB is always (apart from the case of 1040+123, for

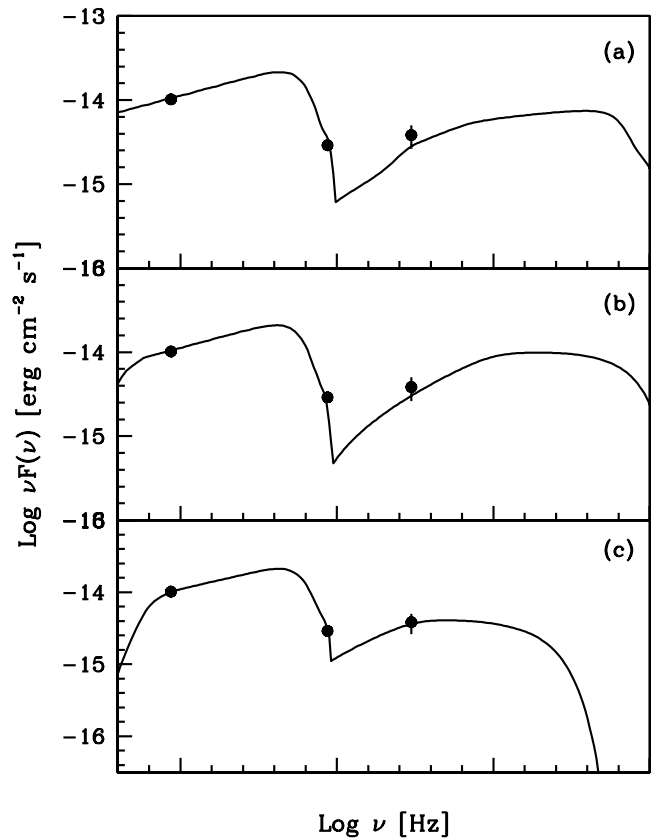


FIG. 2.—SED of 0405–123 with the result of the synchrotron + IC model assuming (a) a radius corresponding to an angular scale of  $1''$ , (b) the radius estimated from the size of the most compact component visible in VLA maps, and (c) equipartition and a very compact source (see text for more details).

which the discrepancy was much smaller to start with) 1 or 2 orders of magnitude below the equipartition value.

In order to approach equipartition, extremely compact hot spots would be needed, with sizes of the order of tens of parsecs or even smaller. As an example, we reproduced the observed SED of 0405–123 *imposing equipartition*. A radius  $R \sim 5 \times 10^{18}$  cm ( $\sim 1$  pc) is required, and the corresponding SED is shown in Figure 2c. We consider this possibility quite unlikely: for instance, the size of the hot spot in Cyg A, estimated from radio measurements, is of the order of 2 kpc (Carilli & Barthel 1996).

The only way to reconcile the extreme compactness of the emission region, needed to reach equipartition, with the observed larger sizes of the hot spots is to suppose that the emission region is strongly clumped. Several very small ( $R \sim 10^{17}$  cm) emission sites embedded in some confining medium would be needed (see Appendix B). The compact emission regions could correspond to reconnection sites, where particles are energized by the dissipation of the magnetic field (e.g., Lyutikov 2003). However, this explanation is rather speculative, and we consider there to be little evidence for such extreme clumping.

### 3.2. Beaming

So far, we have considered the emitting plasma within the hot spot to be at rest. Indeed, the advance speeds usually inferred for the head of the jet are subrelativistic ( $v \sim 0.1c$ ; e.g., Liu et al. 1992). On the other hand, the plasma flowing into the hot spot could well be relativistic, and the asymmetry of the hot spot's brightness indicates that beaming should be relevant. In three out of six cases a counter–hot spot is present in the radio map; thus, the overall anisotropy should not be extreme, at least for the radio emission. If the emission process is SSC, the beaming hypothesis would *reduce* the radiation energy density in the jet frame, worsening the equipartition problem. However, for the relatively high redshift sources considered here, the IC process on the CMB can play a role, since its contribution is amplified by a factor of  $\Gamma^2$  (Dermer 1995), where  $\Gamma$  is the bulk Lorentz factor of the moving plasma (see also Kataoka et al. 2003).

Again assuming equipartition, we can derive the necessary Doppler factors  $\delta$ , where  $\delta = \Gamma^{-1}(1 - \beta \cos \theta)^{-1}$ , with  $\beta = v/c$  as the plasma speed and  $\theta$  as the angle to the line of sight. The parameters we obtain are reported in Table 3. For  $R = 1''$  the inferred Doppler factors are in the range 3–6. The resulting SEDs are reported in Figure 1 (*solid lines*). For smaller source sizes, larger values of the Doppler factors would be obtained. These derived values predict asymmetries larger than those actually observed in the radio; thus, if the *radio and X-ray emission are produced by the same plasma*, the beaming factor required to ensure equipartition seems too high.

A possible solution is to decouple the radio and X-ray emission, allowing a contribution in the radio from slowly moving plasma to satisfy the hot spot/counter–hot spot constraint, while the X-rays could come from Comptonization of the CMB photons within a portion of the flow still in motion with relativistic speed ( $\delta \sim 3$ –6). A scenario along this line was proposed by Georganopoulos & Kazanas (2003), where the emission is produced in the terminal, slowing down (but still relativistic) portion of the jet. In their model, an important role is played by effects due to the differential beaming of the different regions, which provide, at low  $z$ , the “missing seed photons” necessary for the IC mechanism to produce the observed large X-ray flux. Different portions of the jet emit synchrotron and IC emission with different typical frequencies, and the observed emission is a convolution of these components, each amplified by a different Doppler factor. An alternative possibility is to hypothesize

that the structure of the jet consists of a slow component, the “layer,” producing the radio emission and a fast flow, the “spine,” responsible for the X-ray emission (e.g., Ghisellini et al. 2005). In general, the emission from such a structure would be a “mixture” of IC/CMB and “internally beamed” photons. In the sources analyzed here, located at relatively large  $z$ , the CMB likely dominates over the internal radiation. We note that the Doppler factors derived above, although not consistent with the hot spot/counter–hot spot ratio observed in some of the sources, are smaller than those found in the same jets (e.g., Paper I), consistent with a decelerating flow.

### 3.3. The Hot Spot(s) of 0836+299

For the nearby radio galaxy 0836+299, which shows a quasi-symmetric morphology, we detect X-ray emission from the hot spots on both sides of the nucleus (labeled B and C).

The SED of hot spot B is clearly consistent with a unique emission component from the radio to the X-rays, with a cut-off beyond the X-ray band. For knot C, discussed in detail by van Breugel et al. (1986), the optical emission includes a contribution by line-emitting material of the host galaxy, probably heated by the collision with the propagating jet. We thus use the observed flux as an upper limit to the actual value of the non-thermal flux. The two features are modeled in a similar way. Assuming equipartition, the physical quantities can be uniquely determined. The derived parameters are reported in Table 3 (for  $1''$  size). In both cases the slope of the electron energy distribution has been derived from the radio spectral index, while the value of  $\gamma_{\min}$  has been (arbitrarily) fixed to 10.

## 4. DISCUSSION AND CONCLUSIONS

We investigated the multiwavelength observations of the terminal hot spots detected in several of the jets of the Sambruna et al. (2004) jet survey. For a subgroup of them (eight), for which data are available in three energy bands (radio, optical, and X-rays), we were able to investigate in detail the origin of the broadband emission.

For the six hot spots in powerful FR II quasar jets, the concave shape of the SEDs suggests that the IC mechanism is responsible for the X-ray emission in most of the sources. We first reproduced the SEDs of these hot spots with a one-zone synchrotron + IC model and negligible beaming, finding that equipartition would be largely violated unless the emission region is composed by several extremely small condensations. Our results add to previous analyses (e.g., Hardcastle et al. 2002, 2004; Kataoka et al. 2003; Kino & Takahara 2004) already reporting numerous cases of hot spots out of equipartition when the multi-band emission is modeled with a similar synchrotron + IC model. A possible conclusion is to simply admit that hot spots are quite far from equilibrium and thus the minimum energy condition is not reached.

However, the one-sidedness of some of the hot spots detected at X-rays indicates that relativistic beaming should play a role. If the hot spot plasma flow is still relativistic, the beamed CMB photons can provide the energy density necessary to produce the observed X-ray flux in equipartition conditions, as in the model advanced to explain the emission of jet knots (Tavecchio et al. 2000). In this single-zone model the derived Doppler factors ( $\delta = 3$ –6) seem rather large to be reconciled with the moderate asymmetry observed in the radio.

A way out is to admit that the radio and X-ray fluxes are not produced by the same plasma, i.e., to adopt multizone models, with different plasma speeds for different regions. An interesting scenario was proposed by Georganopoulos & Kazanas

(2003), where the emission is produced in the terminal, slowing down (but still relativistic) portion of the jet. A second possibility is to invoke a structured jet with a fast spine surrounded by a slow layer (e.g., Laing 1993; Chiaberge et al. 2000; Ghisellini et al. 2005). In the hot spot case the initial part of the cocoon, where plasma moves (slowly) back toward the core, could provide an isotropic contribution to the radio flux. However, given the intrinsic dependence of these models on an increased number of parameters, a more quantitative analysis is beyond the scope of this paper.

It is interesting to note that elements supporting the idea that X-ray and radio emission could be associated with different portions of the flow are provided by the morphology observed in some sources. In this respect, the peculiar structures of the terminal jets of 3C 273 (Sambruna et al. 2001; Marshall et al. 2001) and 1136–125 (belonging to the sample of Paper I, but not included in this work because of the nonclear X-ray detection of its radio hot spot) are rather suggestive. Indeed, in both sources the X-ray emission disappears before the end of the jet, being negligible at the hot spot, while the radio luminosity increases continuously and reaches the maximum corresponding to the hot spot. This structure can be interpreted as being due to the progressive deceleration of the flow (Sambruna et al. 2001, 2004; Georganopoulos & Kazanas 2004). Due to the limited spatial resolution in the X-rays, the same sources, observed at a larger distance and/or at a smaller angle to the line of sight, or intrinsically shorter, would show almost coincident X-ray and radio emission, such as those analyzed here, and similar SEDs. The case of 1354+195 could be an example of “marginal” resolution.

A last possibility to account for the observed bright X-ray emission under equipartition conditions, not considered in detail in this paper, would be to assume that the broadband emission is produced through synchrotron radiation by some special electron distribution with an excess of high-energy electrons with respect a standard power law, or, alternatively, by two distinct electron populations. Although this scenario deserves attention (e.g., Harris et al. 2004), some of the models proposed so far need special physical conditions (Dermer & Atoyan 2002) or have difficulties in reproducing in detail the SEDs of the hot spots, in particular around the low optical emission (Stawarz et al. 2004). Different electron populations, as derived, e.g., in some hadronic models (e.g., Mannheim & Biermann 1989), could also contribute to the observed X-ray emission. Clearly, deeper multifrequency observations are needed to better clarify these issues.

The hot spots of the FR I galaxy 0836+299 show SEDs consistent with a single synchrotron component from the radio band to the X-rays. The emission can be produced by synchrotron

radiation from an electron distribution with a maximum Lorentz factor  $\gamma_{\max} \sim 10^7$  in equipartition with the magnetic field. A similar scenario is found in the hot spots of a few other sources (3C 390.3 [Harris et al. 1998], 3C 403 [Hardcastle et al. 2004], B2 0738+313 [Siemiginowska et al. 2003], and 3C 280 [Donahue et al. 2003]), where similarly the X-ray emission is interpreted as the high-energy tail of synchrotron radiation, implying electrons with very high Lorentz factors  $\gamma_e \sim 10^7$ .

We note that these extreme energies are not reached by the electrons accelerated in the hot spots of powerful jets, where the maximum Lorentz factor is around  $10^5$  (Table 3). These findings are consistent with a similar result of Hardcastle et al. (2004), who suggested a possible trend between the power of the source and the maximum energy reached by the electrons. This behavior is reminiscent of the “sequence” displayed by the blazar jets (Fossati et al. 1998), which show a similar trend between the radiated power and the maximum frequency of the synchrotron emission. In both cases the existence of such a trend could be interpreted as the result of the competition between acceleration and cooling processes acting on the electrons (Ghisellini et al. [1998] and Brunetti et al. [2003] for blazars and hot spots, respectively). Better multiwavelength observations (especially in the critical optical–IR region) of hot spots belonging to sources with different powers will clearly be important to confirm this and guide an understanding of the different physical conditions of the terminal jets of FR I and FR II radio galaxies.

We thank G. Brunetti for useful discussions and the anonymous referee for constructive comments. R. C., F. T., and L. M. acknowledge support from grants COFIN-2002-027145-007 and COFIN-2003-027534-004. This project is funded by NASA grant HST-GO-12110A, which is operated by AURA, Inc., under NASA contract NAS 5-26555, and by grant NAS 8-39073 (R. M. S.). Moreover, R. M. S. gratefully acknowledges support from an NSF CAREER award and from the Clare Boothe Luce Program of the Henry Luce Foundation. This work was supported in part by NASA grant NAG 5-12873 and NASA grant GO 2-3195C (C. C. C.) from the Smithsonian Observatory HST-GO-09122.08-A (C. C. C.). Analysis of the radio and optical data was done while C. C. C. attended Brandeis University. Radio astronomy at Brandeis is supported by the NSF. The National Radio Astronomy Observatory is operated by Associated Universities, Inc., under a cooperative agreement with the National Science Foundation. MERLIN is a National Facility operated by the University of Manchester at Jodrell Bank Observatory on behalf of PPARC.

## APPENDIX A

### THE EQUIPARTITION MAGNETIC FIELD

The equipartition magnetic field is derived from the relation

$$\frac{B_{\text{eq}}^2}{8\pi} = U_e = m_e c^2 \int_{\gamma_{\min}}^{\gamma_{\max}} N(\gamma)(\gamma - 1) d\gamma, \quad (\text{A1})$$

where  $N(\gamma) = K\gamma^{-n}$  is the electron energy distribution. To find the value of  $B_{\text{eq}}$ , equation (A1) has to be coupled with the expression for the synchrotron luminosity. A simple expression for  $B_{\text{eq}}$  can be derived using the expression for the specific synchrotron luminosity (e.g., Ghisellini & Maraschi 1989),

$$L_s(\nu_s) = c(\alpha)KB^{1+\alpha}V\nu_s^{-\alpha}, \quad (\text{A2})$$

where  $V = (4/3)\pi R^3$  is the volume of the spherical emitting region,  $c(\alpha)$  is a constant, and the luminosity is calculated at the frequency  $\nu_s$ . Considering the case  $\gamma_{\min} \gg 1$  and using equation (A1), one obtains

$$B_{\text{eq}} = \left[ \frac{8\pi m_e c^2 L_s(\nu_s) f}{c(\alpha) \nu_s^{-\alpha} V} \right]^{1/(3+\alpha)}. \quad (\text{A3})$$

The factor  $f$  depends on the details of the electron distribution:

$$f = \frac{1}{n-2} (\gamma_{\min}^{2-n} - \gamma_{\max}^{2-n}). \quad (\text{A4})$$

## APPENDIX B

### REDUCTION OF THE SIZE—CLUMPING

Let us assume that the actual emitting region is composed by  $N$  equal subsources, each one modeled as spheres with volume  $V' = \phi V$  ( $\phi < 1$ ), corresponding to the radius  $R' = \phi^{1/3} R$ , where  $V$  and  $R$  are the volume and the radius at some reference point (e.g., that corresponding to the size measured at the VLA). Using the results of Appendix A, for each subsource we can calculate the equipartition field,

$$B_{\text{eq}} = \left[ \frac{8\pi m_e c^2 L'_s(\nu_s) f}{c(\alpha) \nu_s^{-\alpha} V'} \right]^{1/(3+\alpha)} = B_{\text{eq}}^* (\phi N)^{1/(3+\alpha)}, \quad (\text{B1})$$

where  $L'_s(\nu_s) = L_s(\nu_s)/N$  is the fraction of the total synchrotron emission produced by each subsource and  $B_{\text{eq}}^*$  is the equipartition field calculated for the standard source with radius  $R$ .

On the other hand, the magnetic field necessary to produce the observed synchrotron to SSC luminosity ratio can be estimated from equation (A2) and the corresponding approximated equation for the SSC luminosity (e.g., Ghisellini & Maraschi 1989),

$$L_c(\nu_c) = b(\alpha) K^2 B^{1+\alpha} V' R' \nu_c^{-\alpha}, \quad (\text{B2})$$

from which we can derive

$$B = B^* \phi^{-2/(3+3\alpha)} N^{-1/(1+\alpha)}, \quad (\text{B3})$$

where  $B^*$  is the magnetic field for the reference source. Therefore, the ratio between the magnetic field and the equipartition magnetic field can be expressed as

$$\frac{B}{B_{\text{eq}}} = \frac{B^*}{B_{\text{eq}}^*} \phi^{-a} N^{-b}, \quad (\text{B4})$$

where

$$a = \frac{3-\alpha}{3(1+\alpha)(3+\alpha)}, \quad b = \frac{2}{(1+\alpha)(3+\alpha)}. \quad (\text{B5})$$

The “filling factor”  $\eta$  of the source would be

$$\eta = \frac{\sum_N V'}{V} = N\phi. \quad (\text{B6})$$

## REFERENCES

- Begelman, M. C., & Cioffi, D. F. 1989, *ApJ*, 345, L21  
 Bennett, C. L., et al. 2003, *ApJS*, 148, 1  
 Blandford, R. D., & Rees, M. J. 1974, *MNRAS*, 169, 395  
 Bridle, A. H., Hough, D. H., Lonsdale, C. J., Burns, J. O., & Laing, R. A. 1994, *AJ*, 108, 766  
 Brunetti, G., Mack, K.-H., Prieto, M. A., & Varano, S. 2003, *MNRAS*, 345, L40  
 Brunetti, G., Setti, G., & Comastri, A. 1997, *A&A*, 325, 898  
 Carilli, C. L., & Barthel, P. D. 1996, *A&A Rev.*, 7, 1  
 Cheung, C. C. 2004, Ph.D. thesis, Brandeis Univ.  
 Chiaberge, M., Celotti, A., Capetti, A., & Ghisellini, G. 2000, *A&A*, 358, 104  
 Cox, C. I., Gull, S. F., & Scheuer, P. A. G. 1991, *MNRAS*, 252, 558  
 Dermer, C. D. 1995, *ApJ*, 446, L63  
 Dermer, C. D., & Atoyan, A. M. 2002, *ApJ*, 568, L81  
 Donahue, M., Daly, R. A., & Horner, D. J. 2003, *ApJ*, 584, 643  
 Feigelson, E. D., Laurent-Muehleisen, S. A., Kollgaard, R. I., & Fomalont, E. B. 1995, *ApJ*, 449, L149  
 Fossati, G., Maraschi, L., Celotti, A., Comastri, A., & Ghisellini, G. 1998, *MNRAS*, 299, 433  
 Georganopoulos, M., & Kazanas, D. 2003, *ApJ*, 589, L5  
 ———. 2004, *ApJ*, 604, L81  
 Ghisellini, G., Celotti, A., Fossati, G., Maraschi, L., & Comastri, A. 1998, *MNRAS*, 301, 451  
 Ghisellini, G., & Maraschi, L. 1989, *ApJ*, 340, 181  
 Ghisellini, G., Tavecchio, F., & Chiaberge, M. 2005, *A&A*, 432, 401

- Hardcastle, M. J., Birkinshaw, M., Cameron, R. A., Harris, D. E., Looney, L. W., & Worrall, D. M. 2002, *ApJ*, 581, 948
- Hardcastle, M. J., Harris, D. E., Worrall, D. M., & Birkinshaw, M. 2004, *ApJ*, 612, 729
- Harris, D. E., Carilli, C. L., & Perley, R. A. 1994, *Nature*, 367, 713
- Harris, D. E., & Krawczynski, H. 2002, *ApJ*, 565, 244
- Harris, D. E., Leighly, K. M., & Leahy, J. P. 1998, *ApJ*, 499, L149
- Harris, D. E., Mossman, A. E., & Walker, R. C. 2004, *ApJ*, 615, 161
- Hummel, C. A., et al. 1992, *A&A*, 257, 489
- Kataoka, J., Edwards, P., Georganopoulos, M., Takahara, F., & Wagner, S. 2003, *A&A*, 399, 91
- Kino, M., & Takahara, F. 2004, *MNRAS*, 349, 336
- Laing, R. A. 1993, in *Proc. STScI Symp. 6* (1993 May), *Astrophysical Jets*, ed. D. Burgarella, M. Livio, & C. P. O'Dea (Cambridge: Cambridge Univ. Press), 95
- Liu, R., Pooley, G., & Riley, J. M. 1992, *MNRAS*, 257, 545
- Lytikov, M. 2003, *NewA Rev.*, 47, 513
- Mannheim, K., & Biermann, P. L. 1989, *A&A*, 221, 211
- Marshall, H. L., et al. 2001, *ApJ*, 549, L167
- Sambruna, R. M., Gambill, J. K., Maraschi, L., Tavecchio, F., Cerutti, R., Cheung, C. C., Urry, C. M., & Chartas, G. 2004, *ApJ*, 608, 698 (Paper I)
- Sambruna, R. M., Urry, C. M., Tavecchio, F., Maraschi, L., Scarpa, R., Chartas, G., & Muxlow, T. 2001, *ApJ*, 549, L161
- Scheuer, P. A. G. 1974, *MNRAS*, 166, 513
- Siemiginowska, A., et al. 2003, *ApJ*, 595, 643
- Stawarz, Ł., Sikora, M., Ostrowski, M., & Begelman, M. C. 2004, *ApJ*, 608, 95
- Tashiro, M., Makishima, K., Iyomoto, N., Isobe, N., & Kaneda, H. 2001, *ApJ*, 546, L19
- Tashiro, M., et al. 1998, *ApJ*, 499, 713
- Tavecchio, F., Maraschi, L., Sambruna, R. M., & Urry, C. M. 2000, *ApJ*, 544, L23
- van Breugel, W. J. M., Heckman, T. M., Miley, G. K., & Filippenko, A. V. 1986, *ApJ*, 311, 58